MASSACHUSETTS INSTITUTE OF TECHNOLOGY
LINCOLN LABORATORY

PHASED-ARRAY CALIBRATION BY ADAPTIVE NULLING

H.M. AUMANN
F.G. WILLWERTH
Group 61

TECHNICAL REPORT 915

20 MAY 1991

LEXINGTON MASSACHUSETTS

ABSTRACT

The limitations to ultra-low sidelobe performance are explored using a 32-element linear array, operating at L-band, containing transmit/receive (T/R) modules with 12-bit attenuators and 12-bit phase shifters. With conventional far-field calibrations, the average sidelobe level of the array was about -40 dB. In theory, considerably lower sidelobe performance is expected from such an array.

Initially, sidelobe performance was thought to be limited by inadequate calibrations. An examination of individual array element patterns showed a mirror-symmetric ripple which could only be attributed to edge effects in a small array. Simulations indicated that more precise calibrations would not compensate for these element-pattern differences.

An adaptive calibration technique was developed which iteratively adjusted the attenuator and phaser commands to create nulls in the antenna pattern in the direction of the nulls of a theoretical antenna pattern. With adaptive calibrations, the average sidelobe level can be lowered to -60 dB. The technique can be used for interference suppression by implementing antenna patterns with deep nulls in specified directions.

TABLE OF CONTENTS

LIST OF ILLUSTRATIONS

1. INTRODUCTION

One of the main advantages of a phased array is low sidelobe performance. Low sidelobes are beneficial for both clutter and interference suppression. However, aside from limitations due to measurement range and multipath effects, low sidelobe performance can be difficult to achieve for many reasons.

Quantization effects are often claimed to limit array sidelobe performance. The phased array described in this report contained 12-bit attenuators and phase shifters; quantization errors should be insignificant.

It is desirable to build array components with sufficiently tight tolerances to make further alignment or calibrations unnecessary. In practice, amplitude and phase differences in the T/R modules and transmission lines of the beamforming network are almost unavoidable. Array calibrations are commonly used to compensate for these differences; however, the calibrations may not be satisfactory if they are based on an inadequate array model.

Array element patterns are assumed to be uniform. Mutual coupling and edge effects may distort array element patterns, thus compromising the array calibrations and excitation-function calculations. Standard array calibrations cannot compensate for element-pattern differences.

Rather than attempting to minimize the various error sources, the phased-array calibration technique described in this report concentrates on achieving the lowest possible sidelobe performance under the given conditions.

2. ANTENNA RANGE AND PHASED-ARRAY CHARACTERISTICS

2.1 Antenna Test Range

Phased-array calibrations and antenna-pattern measurements were carried out using the linear array shown in Figure 1 on a 100-ft. ground-reflection antenna range, shown in Figure 2. The range geometry is shown in Figure 3; knowledge of the range and array dimensions is essential to the alignment process.

The antenna range did not meet the conventional far-field criterion given by $2D^2/\lambda$. This formula limits the maximum phase distortion at the face of the array to 22.5 degrees. For the test array with a source at 100 ft., the maximum phase distortion is 75 degrees. In either case, focusing the array will be necessary. The alignment process described in this report automatically includes array focusing.

2.2 Phased-Array Characteristics

The experimental array, operating at L-band, measured 15 ft. by 2 ft. and contained 36 identical waveguide-radiating elements. Two elements on either end of the array were terminated to reduce edge effects. The remaining 32 elements were connected to T/R modules.

Half-height, open-ended waveguide-radiating elements were chosen primarily because they are inexpensive and have a broad, aspect-angle-insensitive radiation pattern. Typical element patterns are shown in Figure 4. In the center of the array, the element patterns were nearly identical; however, at the ends of the array the element patterns exhibited a mirror-symmetric ripple that was attributed to edge diffraction.

Array alignment is usually performed with the array at broadside. Each array element is then examined individually and the array insertion attenuation and phase are adjusted until the broadside response of all elements is the same. This can be achieved at any specific angle; however, at any other angle, comparison of the element patterns in Figure 4 suggests that the insertion attenuation might be 2-3 dB in error. Thus, standard array calibrations cannot compensate for differences in the element patterns.

Good sidelobe performance in a small array requires T/R modules with very precise attenuation and phase control. In the past, array sidelobe performance at L-band was usually limited by quantization effects in the T/R modules. Commonly available L-band attenuators and phase shifters are limited to 5-6 bits of control; however, each module in the test array had 12 bits of amplitude and phase control. This was achieved by using voltage-controlled devices operating at an intermediate frequency [1]. Typical characteristics are shown in Figures 5 and 6. A nominal quadratic approximation adequately described the attenuator and phaser characteristics. There is a weak attenuator and phaser interaction; a change in attenuation will result in a significant change in phase, and vice versa. This interaction is not easily accounted for by a closed-form expression; however, it is corrected by the iterative alignment technique.

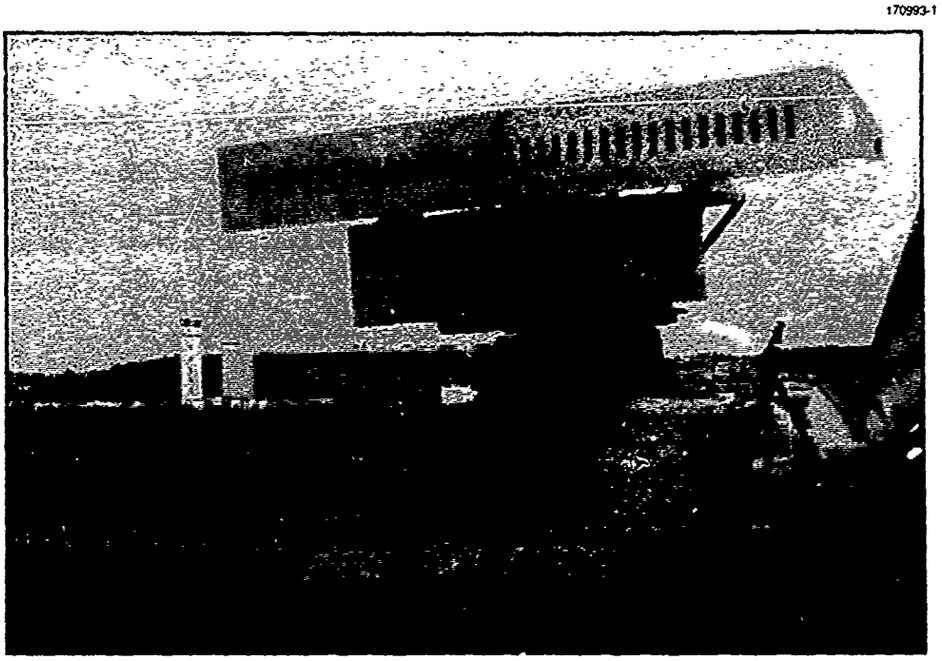

Figure 1. Experimental phased array.

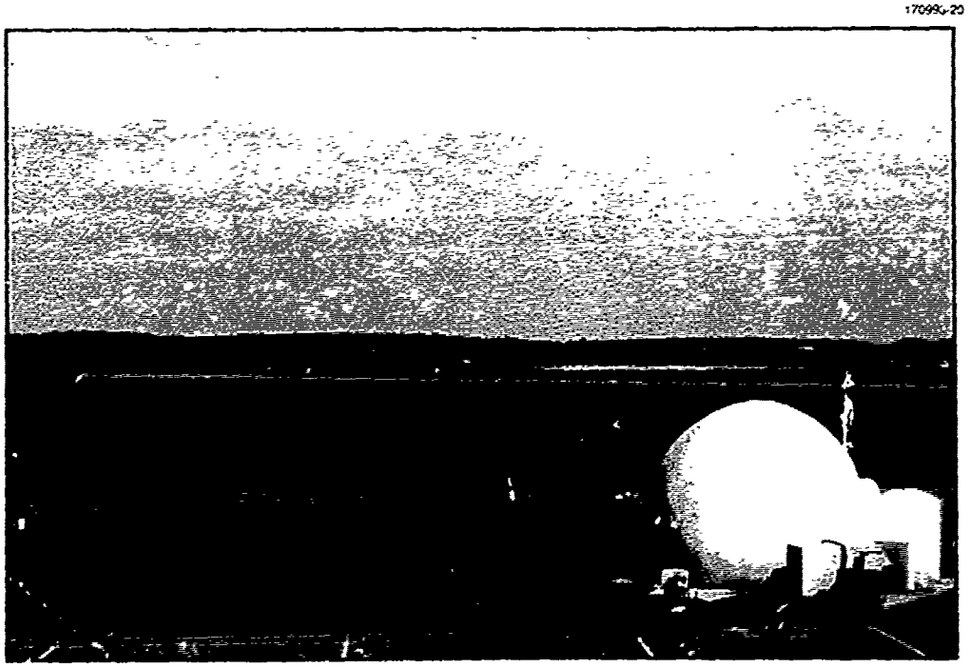

Figure 2. Antenna test range.

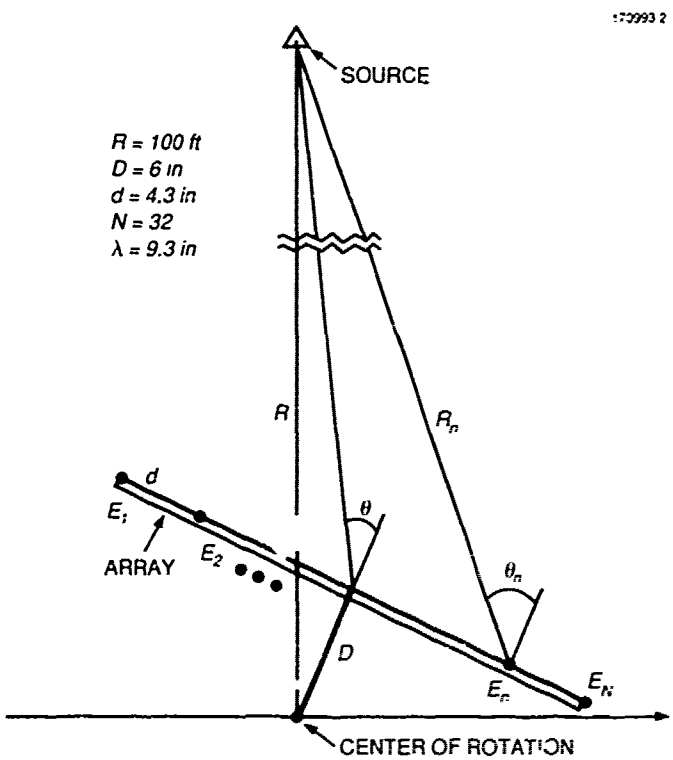

Figure 3. Antenna range geometry.

2.3 Performance with Standard Calibrations

The standard array calibrations described in Section 2.2 were carried out with the array at broadside: all active elements were terminated and the characteristics of each element were determined. An example of an antenna pattern with such calibrations is given in Figure 7. Although the measured average sidelobe level of -39 dB was considered quite good, with 12-bit quantization the sidelobe level should have been -45 dB.

One way of determining the limits of array sidelobe performance is to measure the average sidelobe level as increasingly severe array tapers are commanded. Figure 8 shows that with standard calibrations the array sidelobe performance was limited to about -40 dB.

A simulation was carried out using measured element patterns as shown in Figure 4. The actual element patterns included range multipath as well as small array effects. Perfectly implemented excitation functions were assumed: starting with standard calibrations, the excitation functions were applied with numerical precision. A typical simulated antenna pattern is shown in Figure 9. The resulting array sidelobe performance in Figure 8 was only a few dB better than the array performance measured on the antenna range, indicating that the standard calibrations were as good as could be expected.

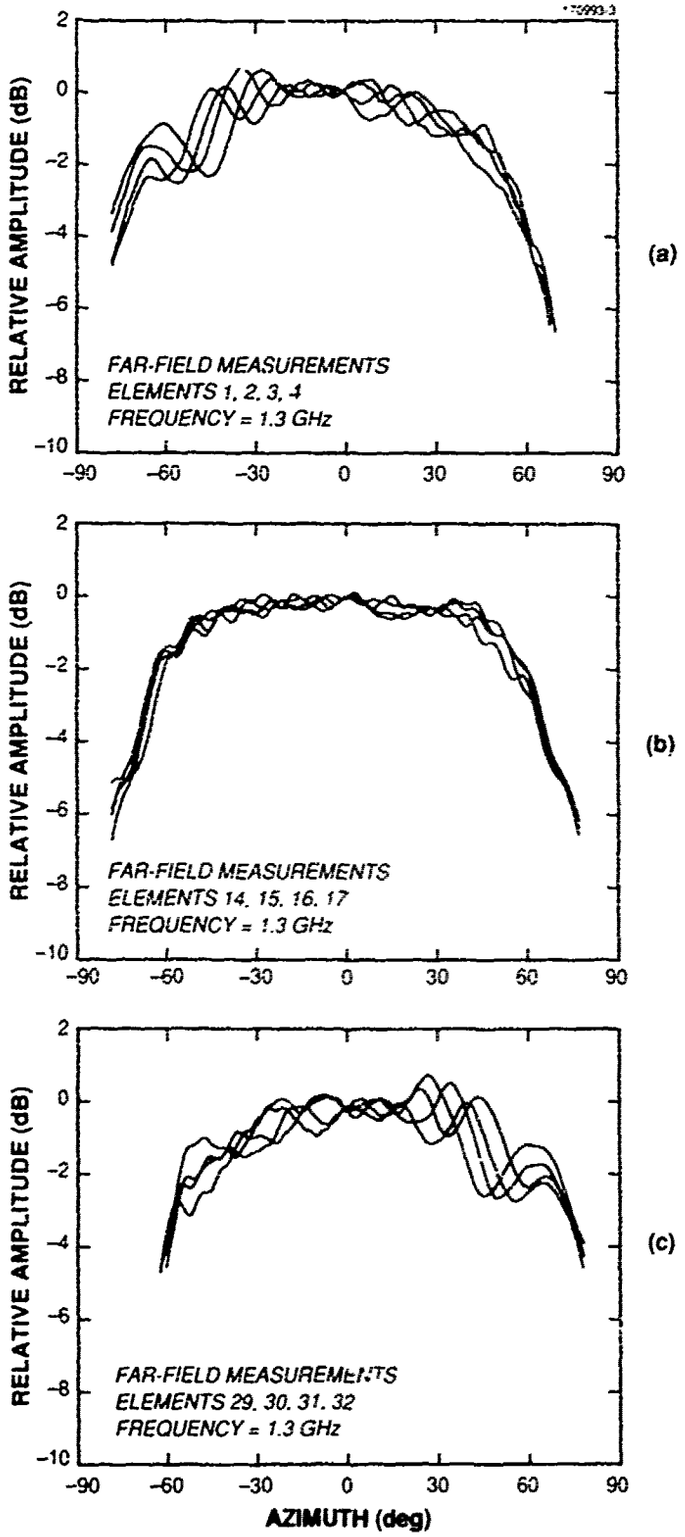

Figure 4. Typical array element patterns.

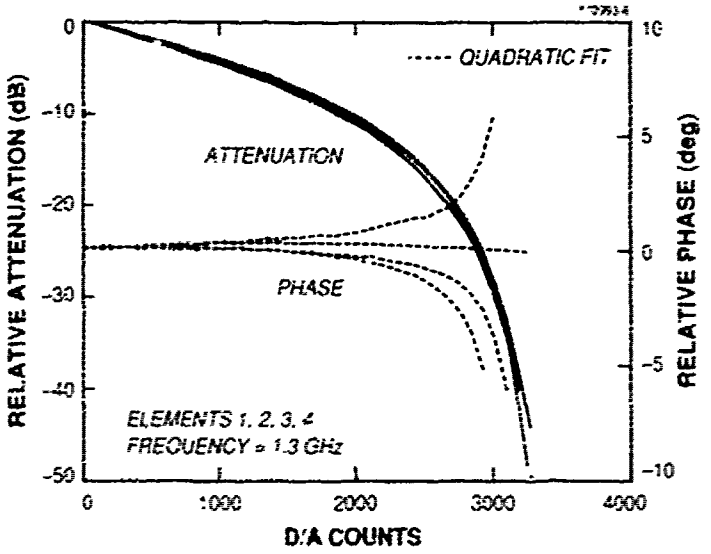

Figure 5. Typical attenuator characteristics.

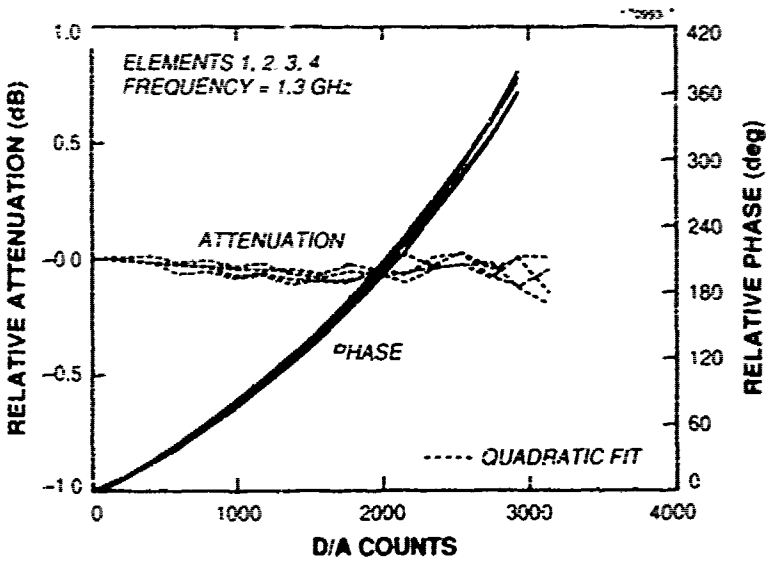

Figure 6. Typical phaser characteristics.

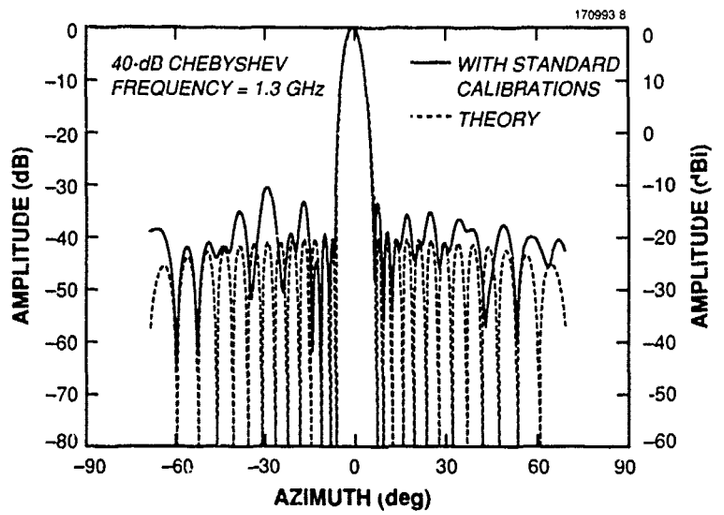

Figure 7. Measured antenna pattern with standard calibrations.

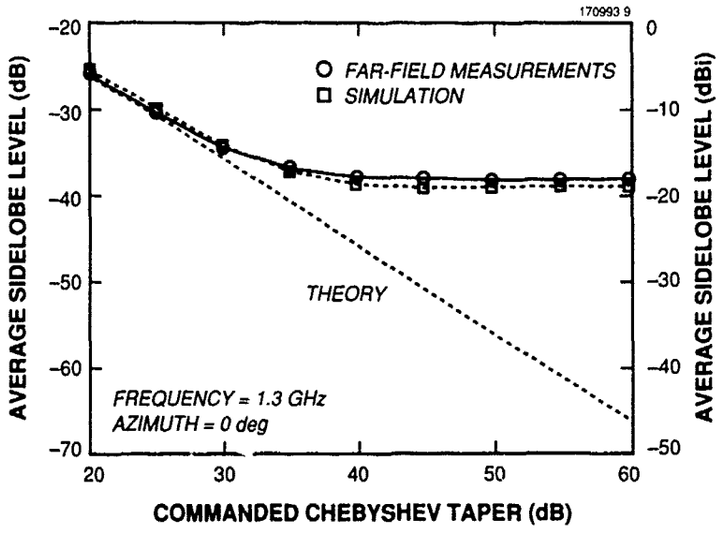

Figure 8. Array sidelobe performance with standard calibrations.

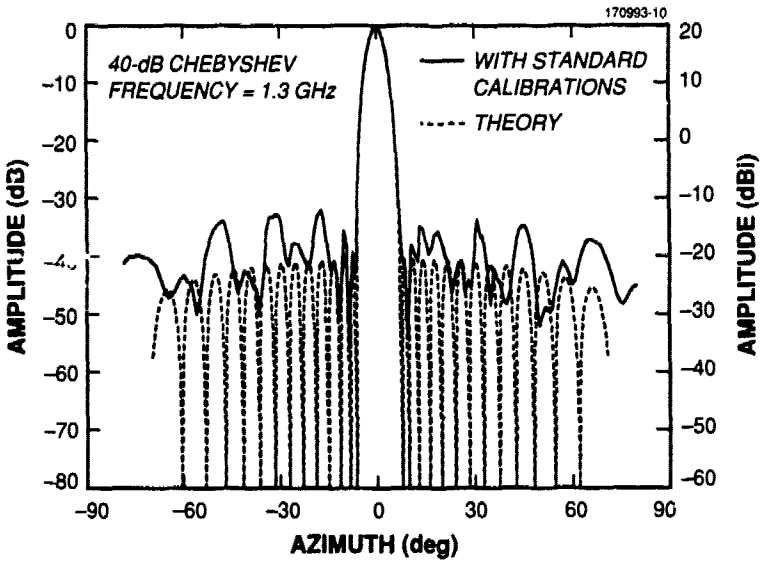

Figure 9. Simulated antenna pattern with standard calibrations.

3. ADAPTIVE CALIBRATION TECHNIQUE

A technique for calibrating a phased array from the far-field pattern has been described by Patton [2]. The process consists of calculating the far-field pattern of an array by Fourier transformation of planar near-field measurements. The array element excitations are then computed by inverse Fourier transformation of the far-field pattern back to the aperture plane.

The array calibration technique described in this report is based on iteratively forming nulls in the antenna pattern [3]. The calibrations are considered adaptive in that the actual antenna pattern is adjusted to match a theoretical model. When the specified nulls correspond to the nulls of an array with uniform illumination, the technique yields the insertion attenuation and phase of the array elements. By specifying other null directions, different array illumination functions can be implemented.

3.1 Theory

The excitation function of a phased array can be calculated from an observed far-field pattern by the direct matrix-inversion method [4]. The pattern of a linear N-element array in the direction θ is given by

$$P(\theta) = \sum_{n=1}^{N} w_n z_n(\theta) \tag{1}$$

$$z_n(\theta) = \frac{E_n(\theta_n)}{R_n} \exp j\frac{2\pi}{\lambda}(R_n mc \qquad ,$$

where w_n is the complex excitation coefficients and $E_n(\theta_n)$ is the element patterns. All array elements are assumed identical and the range geometry is such that

$$E_1(\theta_1) = E_2(\theta_2) = \cdots = E_n(\theta_n) \qquad . \tag{2}$$

By measuring the antenna pattern in N directions, a set of linear equations can be written and solved for the N excitation coefficients. These equations can be expressed in matrix form as

$$\boldsymbol{W} = \boldsymbol{Z}^{-1}\,\boldsymbol{P} \tag{3}$$

where

$$\boldsymbol{W} = \begin{bmatrix} w_1 \\ w_2 \\ \vdots \\ w_N \end{bmatrix}$$

$$\boldsymbol{Z} = \begin{bmatrix} z_1(\theta_1) & z_2(\theta_1) & \cdots & z_N(\theta_2) \\ z_1(\theta_2) & z_2(\theta_2) & \cdots & z_N(\theta_3) \\ \cdots & \cdots & \cdots & \cdots \\ z_1(\theta_N) & z_2(\theta_N) & \cdots & z_N(\theta_N) \end{bmatrix}$$

$$\boldsymbol{P} = \begin{bmatrix} P(\theta_1) \\ P(\theta_2) \\ \vdots \\ P(\theta_N) \end{bmatrix}$$

In theory, measurements of the antenna pattern in any N directions could be chosen to determine the array-excitation function. In practice, the quality of results obtained from a single "back transformation" has not been satisfactory, as the assumption of identical element patterns is of limited validity and the range geometry is not sufficiently known. Thus, an iterative solution, with careful selection of the measurement directions, will be required.

3.2 Measurement Selection

Any measured antenna pattern will be affected by the specific range geometry. Thus, Figure 3 should be used to carefully calculate the range geometry, specifically focusing corrections. Equation (1) also indicates that differences in the amplitude and phase of individual element patterns and errors in the excitation function have similar effects on the antenna pattern. This interaction can be minimized by making measurements in the directions of the pattern nulls.

For commonly used array tapers, the excitation function can be written in factored form. Consequently, the null locations of the far-field pattern are explicitly known [5]; the null locations were probably used to specify the array sidelobe level. For an N-element array, there can be at most $N-1$ nulls in the antenna pattern. Ideally, if the main lobe is at θ_p and the nulls are at $\theta_1, \theta_2, \cdots, \theta_{N-1}$, then the normalized pattern values are

$$\begin{bmatrix} P(\theta_p) \\ P(\theta_1) \\ \vdots \\ P(\theta_{N-1}) \end{bmatrix} = \begin{bmatrix} 1 \\ 0 \\ \vdots \\ 0 \end{bmatrix} \quad , \tag{4}$$

and the matrix inversion in Equation (3) will return the theoretical excitation function $\boldsymbol{W}_T$.

As a result of the assumption made in Equation (2), the nulls in the antenna pattern are entirely determined by the array factor, and the above calculation will not be affected by the shape of the element patterns.

Because the array-under-test and the measurement range are not perfect, the measured antenna response will not be zero at the null locations; that is,

$$\begin{bmatrix} P(\theta_p) \\ P(\theta_1) \\ \vdots \\ P(\theta_{N-1}) \end{bmatrix} = \begin{bmatrix} 1 \\ \epsilon_1 \\ \vdots \\ \epsilon_{N-1} \end{bmatrix} \quad . \tag{5}$$

However, Equations (5) and (3) can be used to obtain an estimate $\boldsymbol{W}_E$ of the applied excitation function. In the following calibration procedure, attenuation and phase commands will be adjusted until differences between the estimated and theoretical excitation function are at minimum. When this is accomplished, the nulls of the measured and theoretical antenna patterns have been matched.

In general, the sidelobe peaks rather than the nulls of an antenna pattern are of interest. By forcing the antenna pattern to have nulls in the proper directions, a well-formed antenna pattern is virtually assured.

It should be noted that the process is mathematically identical to adaptive nulling by sample matrix inversion [6], in which the array receives a desired signal from a given direction and suppresses undesired signals in $N-1$ carefully specified other directions.

3.3 Calibration Procedure

The first step in phased array calibrations is to correct for element insertion attenuation and phase differences. Initially, an excitation function $\boldsymbol{W}_C$ is commanded without corrections to yield a uniform illumination $\boldsymbol{W}_T$

$$\boldsymbol{W}_C = \boldsymbol{W}_T = \begin{bmatrix} 1 \\ 1 \\ \vdots \\ 1 \end{bmatrix} \quad . \tag{6}$$

The resulting antenna pattern of the uncalibrated test array is shown in Figure 10. The amplitude and phase of the antenna pattern is measured at broadside and at the null locations corresponding to a uniform illumination. An estimate of the applied excitation function $\boldsymbol{W}_E(i)$ is obtained from Equation (3). This estimate is then used to update the commanded excitation function on the next iteration as follows:

$$\boldsymbol{W}_C(i+1) = \boldsymbol{W}_C(i) \left[\frac{\boldsymbol{W}_T}{\boldsymbol{W}_E(i)} \right]^k \quad , \tag{7}$$

where $k \leq 1$ is a gain constant. The actual commands have to be expressed in counts based on nominal attenuator and phaser characteristics. The above process is repeated until

$$\boldsymbol{W}_E(i) \approx \boldsymbol{W}_T \tag{8}$$

and there is no further improvement in the null depths; Figure 11 shows the final antenna pattern. The array element insertion attenuation and phase are given by the reciprocal of $\boldsymbol{W}_C$. The insertion attenuation and phase as determined by standard calibrations and as measured by adaptive calibrations are shown in Figures 12 and 13, respectively. Standard array calibrations are usually carried out with a source at broadside; Figure 3 shows that the element patterns are not identical at all angles. Adaptive calibrations include element pattern differences and therefore yield slightly different calibration results.

In the experiments, the iterative process was stopped when the null depths exceeded 60 dB. For $k = 0.7$ this was usually achieved after five or six iterations. As with any feedback algorithm, there is concern with convergence; for example, an instability may occur if the $\boldsymbol{Z}$-matrix does not adequately model the array and range geometry. Another cause for instability may be a lack of monotonicity in the attenuator and phaser characteristics.

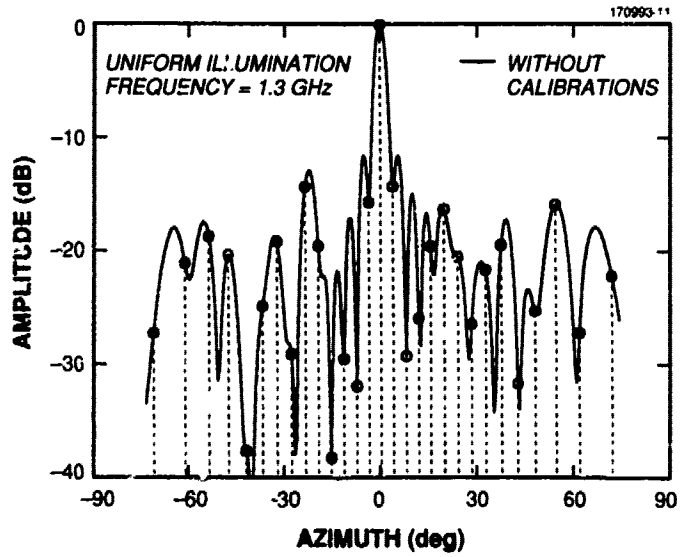

Figure 10. Uncalibrated array pattern.

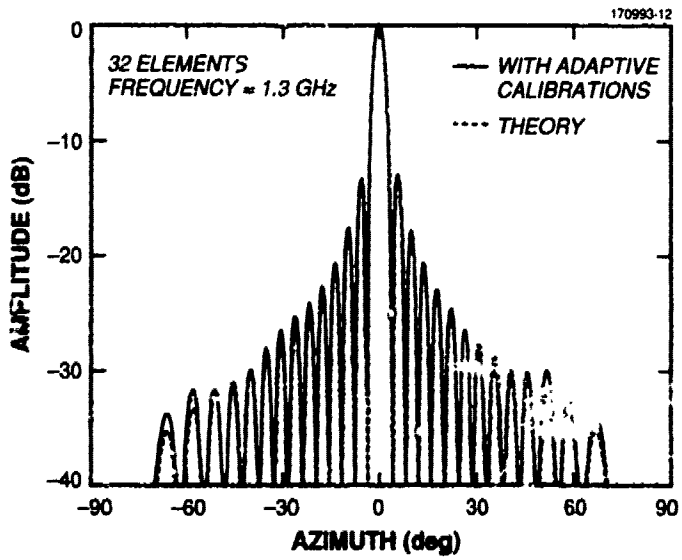

Figure 11. Array pattern with uniform illumination.

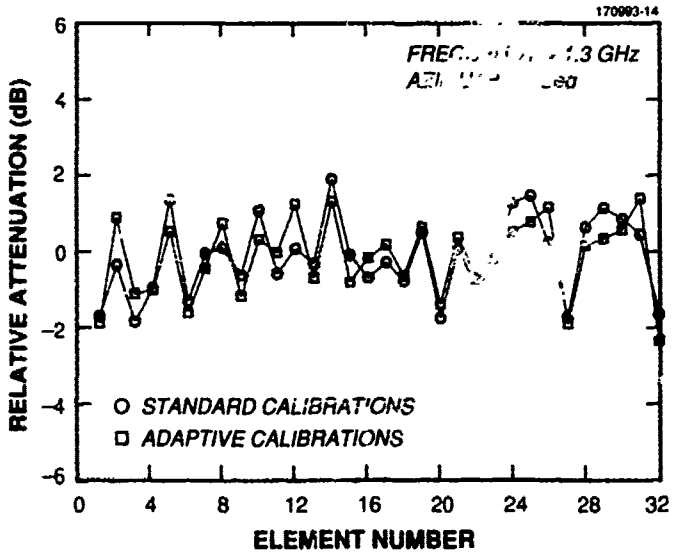

Figure 12. Comparison of insertion attenuation.

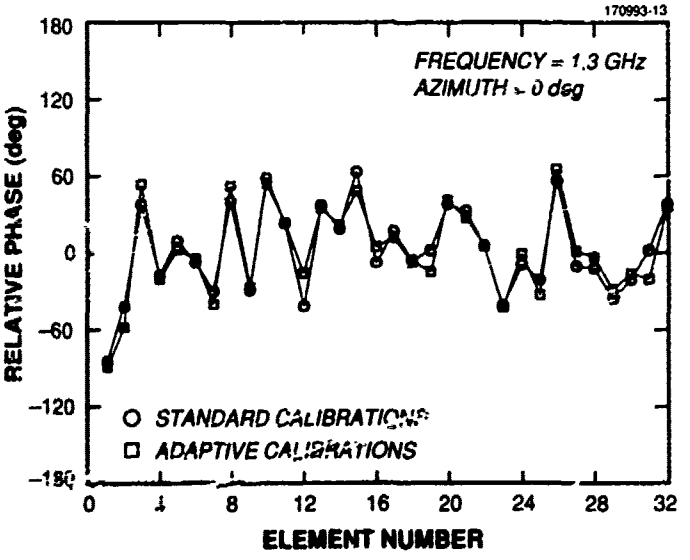

Figure 13. Comparison of insertion phase.

4. PERFORMANCE WITH ADAPTIVE CALIBRATIONS

4.1 Sidelobe Suppression by Chebyshev Taper

The calibration technique is not limited to a uniform illumination. For example, Figure 14 shows the adaptively determined excitation function required to implement a 40-dB Chebyshev taper. A parabolic phase distortion necessary to phase focusing is clearly evident. Although the differences between standard and adaptively determined excitation functions are usually quite small. the resulting array pattern in Figure 15 represents a considerable improvement over the corresponding pattern with standard calibrations shown in Figure 7.

With adaptive calibrations, exceedingly low sidelobe performance can be demonstrated. Figure 16 shows an antenna pattern with a 60-dB Chebyshev taper. At that level, the 40-dB dynamic range of the attenuators becomes the limiting factor.

Figure 17 shows the sidelobe performance with adaptive calibrations. With adaptive calibrations, the array performance comes much closer to the theoretical array performance expected from an array with 12 bits of amplitude and phase control.

4.2 Sidelobe Suppression by Null Placement

In the previous section the antenna pattern null directions were chosen to correspond to a standard Chebyshev taper; this resulted in predictable array performance. However, uniformly low sidelobes may not be required in all applications. Rather than accepting the loss in efficiency and broadening of the mainlobe, selective null placement in the direction of a known interference source may be the preferred approach.

For example, Figure 18 shows an adaptively calibrated array pattern with a 30-dB Chebyshev taper and an additional null at -30 degrees. Again, sidelobes in the direction of the interference have been suppressed by 60 dB.

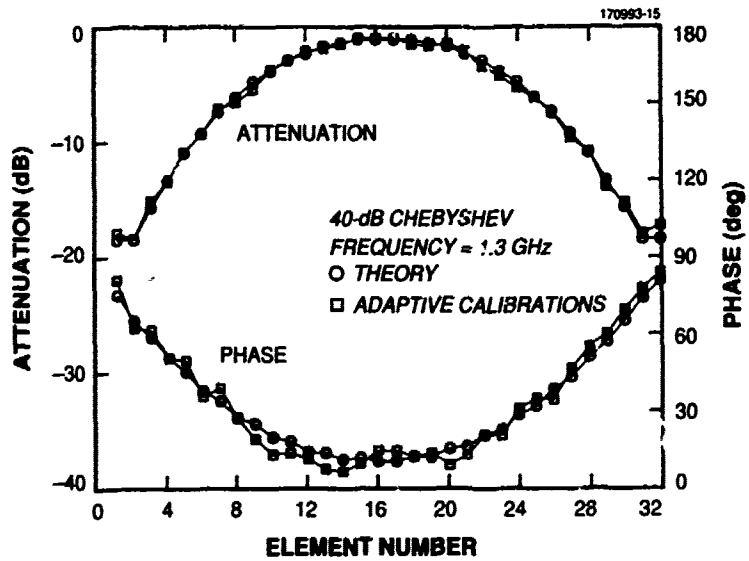

Figure 14. Excitation function for a 40-dB Chebyshev taper.

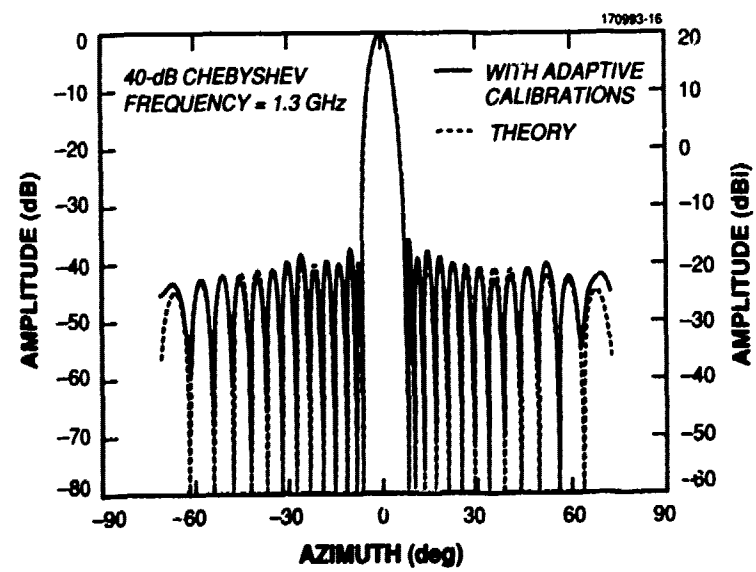

Figure 15. Array pattern with 40-dB Chebyshev taper.

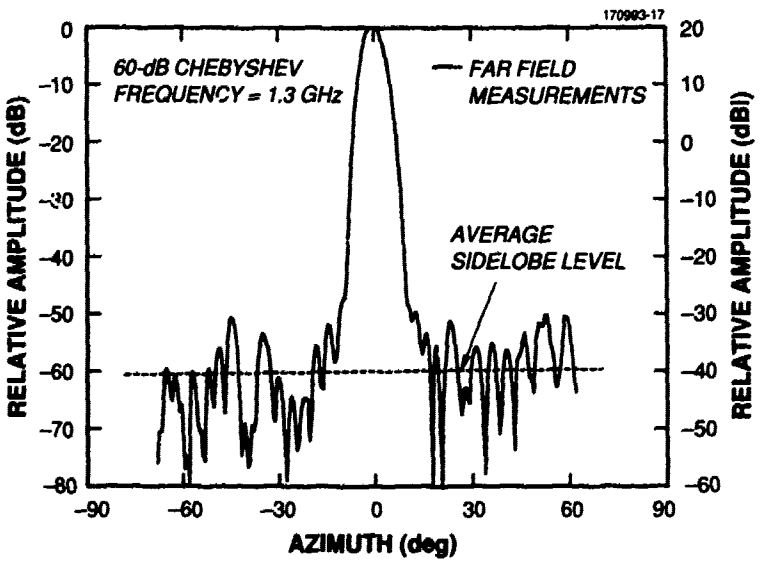

Figure 16. Array pattern with 60-dB Chebyshev taper.

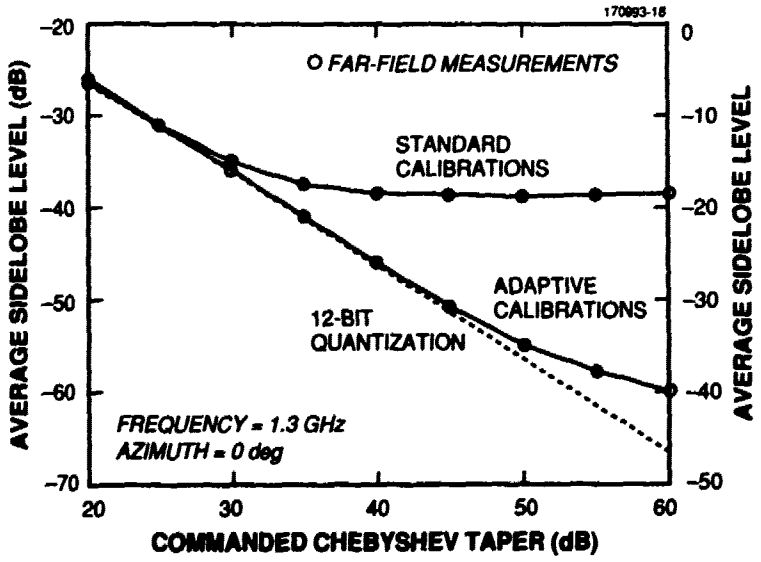

Figure 17. Array sid·lobe performance with adaptive calibrations.

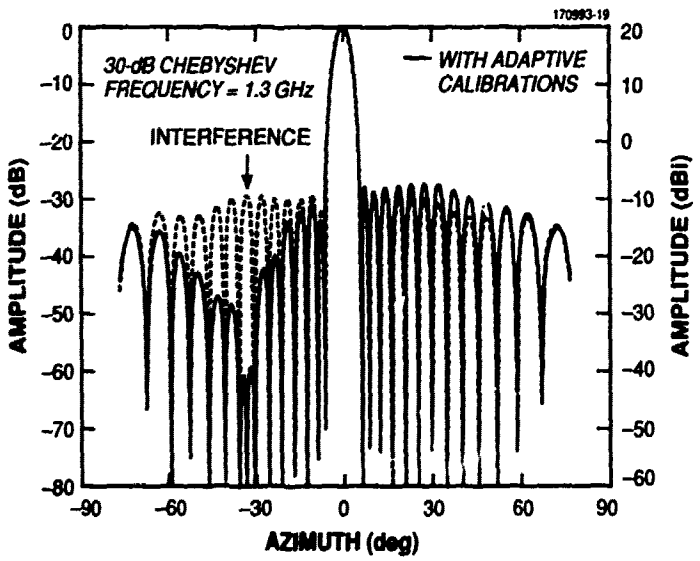

Figure 18. Adaptively calibrated antenna pattern with null.

5. SUMMARY

An adaptive calibration technique for a phased array was described. This technique allows the insertion attenuation and phase of the array elements to be determined directly from the measured far-field pattern. Although not specifically discussed in this report, the technique can readily identify failed T/R modules; no built-in-test capability is required.

The technique is applicable not only to implementing standard array tapers, but also to implementing antenna patterns with deep nulls in specified directions.

REFERENCES

1. H.M. Aumann and F.G. Willwerth, "Intermediate Frequency Transmit/Receive Modules for Low Sidelobe Phased Array Application," 1988 IEEE National Radar Conference Proceedings, Ann Arbor, Michigan.

2. W.T. Patton, "Phased Array Alignment with Planar Near-Field Scanning, or Determining Element Excitation from Planar Near-Field Data," 1981 Antenna Applications Symposium Proceedings, Allerton Park, Illinois.

3. H.M. Aumann and F.G. Willwerth, "F. G. (1989) Measurement of Phased Array Patterns by Near-Field Focusing," 1989 Antenna Measurement and Techniques Conference Proceedings, Monterey, California.

4. M. Hoffman, "The Utility of the Array Pattern Matrix for Linear Array Computations," *IRE Trans. Ant. and Propag.* Vol. AP-9, 97-100 (1961).

5. R.S. Elliot, *Antenna Theory and Design*, Englewood Cliffs, New Jersey: Prentice-Hall (1981). Ch. 5.

6. R.A. Monzingo and T.W. Miller, *Introduction to Adaptive Arrays*, New York: Wiley (1980).

REPORT DOCUMENTATION PAGE

Form Approved
OMB No. 0704-0188

1. AGENCY USE ONLY (*Leave blank*)	2. REPORT DATE	3. REPORT TYPE AND DATES COVERED
	20 May 1991	Technical Report

4. TITLE AND SUBTITLE

Phased-Array Calibration by Adaptive Nulling

5. FUNDING NUMBERS

C — F19628-90-C-0002
P — 227
PE — 63250F

6. AUTHOR(S)

Herbert M. Aumann
Francis G. Willwerth

7. PERFORMING ORGANIZATION NAME(S) AND ADDRESS(ES)

Lincoln Laboratory, MIT
P.O. Box 73
Lexington, MA 02173-9108

8. PERFORMING ORGANIZATION REPORT NUMBER

TR-915

9. SPONSORING/MONITORING AGENCY NAME(S) AND ADDRESS(ES)

AFSSD/XR
P.O. Box 92960
Worldway Postal Center
Los Angeles, CA 90009-2960

10. SPONSORING/MONITORING AGENCY REPORT NUMBER

ESD-TR-91-047

11. SUPPLEMENTARY NOTES

None

12a. DISTRIBUTION/AVAILABILITY STATEMENT

Approved for public release; distribution is unlimited.

12b. DISTRIBUTION CODE

13. ABSTRACT (*Maximum 200 words*)

The limitations to ultra-low sidelobe performance are explored using a 32-element linear array, operating at L-band, containing transmit/receive (T/R) modules with 12-bit attenuators and 12-bit phase shifters. With conventional far-field calibrations, the average sidelobe level of the array was about –40 dB. In theory, considerably lower sidelobe performance is expected from such an array.

Initially, sidelobe performance was thought to be limited by inadequate calibrations. An examination of individual array element patterns showed a mirror-symmetric ripple which could only be attributed to edge effects in a small array. Simulations indicated that more precise calibrations would not compensate for these element-pattern differences.

An adaptive calibration technique was developed which iteratively adjusted the attenuator and phaser commands to create nulls in the antenna pattern in the direction of the nulls of a theoretical antenna pattern. With adaptive calibrations, the average sidelobe level can be lower to –60 dB. The technique can be used for interference suppression by implementing antenna patterns with deep nulls in specified directions.

14. SUBJECT TERMS	15. NUMBER OF PAGES 34
	16. PRICE CODE

17. SECURITY CLASSIFICATION OF REPORT	18. SECURITY CLASSIFICATION OF THIS PAGE	19. SECURITY CLASSIFICATION OF ABSTRACT	20. LIMITATION OF ABSTRACT
Unclassified	Unclassified	Unclassified	SAR